An anatomical atlas-based scaling study for quantifying muscle and hip joint contact forces in above and through-knee amputees using validated musculoskeletal modelling

Diana Toderita, David P. Henson, Christian Klemt, Ziyun Ding, and Anthony MJ Bull

***Abstract* — *Objective:* Customisation of musculoskeletal modelling using magnetic resonance imaging (MRI) significantly improves the model accuracy, but the process is time consuming and computationally intensive. This study hypothesizes that linear scaling to a lower limb amputee model with anthropometric similarity can accurately predict muscle and joint contact forces. *Methods:* An MRI-based anatomical atlas, comprising 18 trans-femoral and through-knee traumatic lower limb amputee models, is developed. Gait data, using a 10-camera motion capture system with two force plates, and surface electromyography (EMG) data were collected. Muscle and hip joint contact forces were quantified using musculoskeletal modelling. The predicted muscle activations from the subject-specific models were validated using EMG recordings. Anthropometry based multiple linear regression models, which minimize errors in force predictions, are presented. *Results:* All predictions showed excellent (error interval c=0–0.15), very good (c=0.15–0.30) or good (c=0.30–0.45) similarity to the EMG data, demonstrating accurate computation of muscle activations. The primary predictors of discrepancies in force predictions were differences in pelvis width ($p<0.001$), body mass index (BMI, $p<0.001$) and stump length to pelvis width ratio ($p<0.001$) between the respective individual and underlying dataset. *Conclusion:* Linear scaling to a model with the most similar pelvis width, BMI and stump length to pelvis width ratio results in modelling outcomes with minimal errors. *Significance:* This study provides robust tools to perform accurate analyses of musculoskeletal mechanics for high-functioning lower limb military amputees, thus facilitating the further understanding and improvement of the amputee's function. The atlas is available in an open source repository.**

***Index Terms* — amputee biomechanics, lower limb musculoskeletal modelling, linear scaling, anatomical atlas**

Manuscript received 15 October 2020; revised 10 February 2021. This work was supported by the Royal British Legion Centre for Blast Injury Studies.

D. Toderita (correspondence e-mail: diana.toderita15@imperial.ac.uk), D. P. Henson, A.M.J. Bull are with the Department of Bioengineering, Imperial College London, SW7 2AZ, UK.

C. Klemt was with the Department of Bioengineering, Imperial College London, SW7 2AZ, UK. He is now with Harvard Medical School and Massachusetts General Hospital, Boston, MA 02114, USA.

Z. Ding was with the Department of Bioengineering, Imperial College London, SW7 2AZ, UK. She is now with the Department of Mechanical Engineering, University of Birmingham, B15 2TT, UK.

I. Introduction

THE Iraq and Afghanistan conflicts have led to 265 major lower limb amputations in the UK military from 2003 to 2014 [1]. Through a rigorous rehabilitation program, this cohort of traumatic amputees achieve high levels of functional performance, with similar physical abilities to those of able-bodied individuals [2], [3]. Return to physical activity is achieved through use of prosthetics and intensive rehabilitation care, which comes at a compensatory cost, as it introduces different muscle recruitment patterns and joint loading profiles, when compared to able-bodied individuals [4]. Based on the loss of joints, muscle mass and normal physiological muscle attachment locations, the overall musculoskeletal function is disrupted, with the degree of disability increasing with increasing levels of amputation. Depending on individual objectives and capabilities, amputees can adopt very distinct movement strategies, which, although beneficial in the short term, can cause detrimental loading of the joints and increased risk of developing comorbidities such as osteoarthritis [5], [6], osteopenia [7] and lower back pain [8] in the long term.

A significant increase in the medial knee joint reaction forces has been reported in the sound limb of unilateral below-knee amputees [4]. This is a result of asymmetrical gait, often observed in unilateral amputees for all levels of amputation, including trans-tibial, trans-femoral and through-knee [9] – [11]. In order to maximise stability during movement and minimize energy consumption and residual limb pain, the amputated side tends to be underloaded, as opposed to the joints of the intact limb, which are overloaded. The increased forces in the medial compartment of the knee are thought to be linked to the high incidence of osteoarthritis in the sound limb of unilateral amputees [5]. Similarly, high occurrence rates of osteopenia on the amputated side have been reported for unilateral above-knee amputees [7] due to the increased reliance on the intact limb and hypothesised inability of the femoral remnant to bear axial loads. However, there is a lack of understanding of the muscle and joint loading patterns in bilateral above and through-knee traumatic amputees. Therefore, there is an immediate need for the investigation of

TABLE I
PARTICIPANT DETAILS

Subject	Age (y)	Body mass (kg)[a]	Calculated intact mass (kg)[b]	Height (cm)[c]	Left amputation level	Left stump length (mm)	Right amputation level	Right stump length (mm)	Prosthetic foot[d]	Prosthetic knee[d]
1	32	86.0	87.5	185	TK[e]	524	TF[f]	399	Triton low profile	Genium
2	27	81.2	84.7	178	TK	343	TF	434	Triton	Genium X3
3	36	90.0	93.9	186	TK	498	TF	328	Triton low profile	Genium X3
4	38	82.5	95.1	180	TF	386	TF	250	Sidekick stubbies[g]	N/A
5	33	89.5	96.8	182	TK	448	TK	479	Triton low profile	Genium
6	32	97.2	102.9	185	TK	485	TK	477	Triton low profile	Genium X3
7	31	68.8	70.8	171	TF	350	TF	359	Triton	Genium X3
8	30	66.7	79.4	175	TF	406	TF	139	Sidekick stubbies	N/A
9	27	76.2	79.8	175	TK	470	TK	464	Sidekick stubbies	N/A

[a] Body mass measured with the prosthetic components.
[b] Calculated according to previous literature [18].
[c] Pre-injury height available from the military records.
[d] All subjects had been using their prosthetic components for a minimum of two years.
[e] TK indicates through-knee amputation.
[f] TF indicates trans-femoral amputation.
[g] Stubbies are foreshortened prostheses with no articulated knee joints.

the kinetic profiles of amputees to allow for the development of solutions which mitigate the risk of developing comorbidities in the long term, and at the same time improve the amputee's functional performance.

Comprehensive descriptions of the mechanical effects of the lower extremity amputation on internal forces during movement can be obtained through musculoskeletal modelling, which requires the subject's anatomical geometry as input. This is usually obtained through the time- and cost-efficient linearly scaled-generic models [12], which allow for geometric variation across subjects through linear scaling, based on the three-dimensional (3D) locations of anatomical landmarks [13]. However, these do not account for inter-individual anatomical variations [14]. Linear scaling to a generic model has been shown to lead to significant errors in force predictions for both upper and lower limb models [15] – [17]. Additionally, amputees have a much wider anthropometric and anatomical variability (and deficit) than able-bodied subjects and so, there are likely to be considerably greater errors in linear scaling from one subject. The accuracy of a musculoskeletal model is strongly dependent on the anatomical geometry (bony landmarks and muscle parameters), which can be obtained from MRI scans. However, the development of subject-specific models is both time and computationally intensive, and furthermore, MRI scans cannot be performed on those military amputees with shrapnel fragments left in the body from the blast injury.

Linear scaling to a musculoskeletal model with anthropometric similarity has been reported to improve the model predictions in muscle and joint contact forces in able-bodied lower [16] and upper extremities [15]. However, there is no existing approach for linear scaling of lower limb amputee musculoskeletal models. In this study, an MRI based anatomical atlas for above and through-knee traumatic amputees was developed and it was hypothesised that linear scaling to a model with anthropometric similarity can predict muscle and joint contact forces with clinically insignificant errors.

II. METHODS

A. Experimental data

This study received approval by the institutional ethics review board. Written consent was obtained from nine bilateral above and through-knee traumatic male amputees (Table I). High resolution MRI scans were obtained using a 3.0T MRI scanner (MAGNETOM Verio, Siemens, Germany) with a 3D T1-weighted spoiled gradient echo sequence with the following settings: 450×450 mm^2 field of view, 1.17×1.17 mm axial plane resolution, 1 mm slice thickness. All subjects were scanned from the top of the iliac crest to the most distal point of the longer residual limb such that both stumps are included in the scans. Therefore, the anatomical atlas consists of two subject-specific unilateral (left and right) models for each study participant.

Gait data were collected from all subjects using a 10-camera VICON motion analysis system (VICON, Oxford Metrics Group, UK) with two force plates (Kistler Type 9286B, Kistler Instrumente AG, Winterthur, Switzerland). Retro reflective markers were placed on 14 anatomical landmarks of the lower limb: left/right anterior and posterior superior iliac spine, medial and lateral sides of the prosthetic knee joint centre of rotation (analogous to the medial and lateral femoral epicondyles), medial and lateral sides of the ankle joint centre of rotation (analogous to the medial and lateral malleoli), second/fifth metatarsal head (placed at the front edge of the foot, above the second/fifth toe), posterior calcaneus (placed on the back of the heel at toe height), midfoot superior (placed on top of the foot, anterior to the pylon base). Additionally, two clusters of three markers each were placed on the thigh

segment (on the lateral side of the prosthetic socket) and shank segment (on the lateral side of the pylon) [19]. All participants performed a static calibration trial, as well as gait trials, which were performed at a self-selected speed. Three successful trials were collected and analysed for each study participant. The marker positions and ground reaction forces were filtered in MATLAB (The Mathworks Inc., Natick, MA, USA) using a zero phase-lag, fourth order Butterworth filter with 6 Hz cut-off frequency prior to model input [20].

Surface EMG (Delsys Incorporated, Natick, MA, USA) was recorded during the gait trials of 6 subjects from the gluteus medius, gluteus maximus, adductor longus and rectus femoris muscles. The raw EMG data were corrected for DC offsets, high-pass filtered at 30 Hz with a fourth order Butterworth filter, full-wave rectified and low pass filtered at 10 Hz [21]. The sensors were positioned to avoid mechanical interference with the prosthetic socket, therefore resulting in different sensor placements than those recommended in the literature [22]. EMG data were not collected for the remaining 3 subjects due to the unfeasible placement of the EMG sensors on the residual limbs.

B. Anatomical geometry

The acquired MRI scans were processed in Mimics (Mimics 19.0, Materialise, Belgium). 2D contours were manually segmented in the axial plane to reconstruct the 3D surfaces of the pelvis, femoral remnant and residual muscles, illustrated in Fig. 1(A). The muscle segmentation procedure has been previously validated using cadaveric measurements, with reported errors of less than 3%, thus demonstrating its reliability [23]. The anterior and posterior superior iliac spine anatomical landmarks were manually digitised on the bone surface. The hip joint centre coordinates were assigned to the coordinates of the centre of a sphere fitted to the femoral head. Additionally, the lines-of-action of 21 muscles (Table II) were described by the origin, via and insertion points [24], all manually digitised in the MRI scans. The origins of the psoas muscle elements, located on the 12th thoracic vertebra (T12), more proximal than the MRI scans, were approximated using the length of the fifth lumbar vertebra and the intervertebral disc. The psoas muscle volume was obtained using a cone approximation, where the cone diameter was the diameter of the psoas muscle in the most proximal available imaging slice and the cone height was represented by the distance between the centre of the psoas muscle's most proximal slice and T12's approximated location. A cylindrical wrapping object was assigned to the iliacus and psoas muscles, which are free to glide over the pubis, and identified in the imaging scans based on the curvature of the muscle lines-of-action. The joint and muscle representations are shown in Fig. 1(B).

Each muscle's physiological cross-sectional area (PCSA) was computed using (1) [25]:

$$\mathrm{PCSA} = \frac{V_m \times \cos\theta}{L_m \times \frac{L_f}{L_m} \times \frac{2.7}{L_s}} \quad (1)$$

The muscle volume, V_m, was obtained from the rendered 3D geometry of each muscle. The muscle length, L_m, was calculated using the 3D Euclidean distance between axial centroids in the MRI scans, in concordance with previous literature [25]. Values for the pennation angle θ, fibre length to muscle length ratio, L_f/L_m, and optimal sarcomere length, L_s, were obtained from cadaveric data [26]. For the muscles not investigated in the literature, θ was set to 0, L_f/L_m to 1 and L_s to 2.7 µm [16], [27].

TABLE II
MUSCLE PARAMETERS OF A REPRESENTATIVE TRANS-FEMORAL AMPUTEE MODEL

Muscle	Muscle group at hip joint	Muscle volume (V_m, cm^3)	Muscle length (L_m, cm)	Fibre length to muscle length ratio (L_f/L_m)	Pennation angle (θ, °)	Sarcomere length (L_s, µm)	PCSA (cm^2)
Adductor brevis	Adductor	143.02	19.23	0.68	6.10	2.91	11.72
Adductor longus	Adductor, Internal rotator	211.92	25.65	0.50	7.10	3.00	18.22
Adductor magnus	Adductor	550.35	38.12	0.39	15.50	2.19	28.94
Biceps femoris long head	Extensor	217.68	32.74	0.28	11.60	2.35	20.24
Gemellus	External rotator	1.54	6.81	1.00	0.00	2.70	0.23
Gluteus maximus	Extensor, External rotator	1174.09	27.78	0.62	21.90	2.60	60.91
Gluteus medius	Abductor, Internal rotator	488.77	19.54	0.37	20.50	2.40	56.29
Gluteus minimus	Abductor, Internal rotator	165.93	12.27	1.00	0.00	2.70	13.52
Gracilis	Adductor	78.54	25.20	0.79	8.20	3.24	4.69
Iliacus	Flexor	311.63	28.28	0.56	14.30	3.02	21.33
Obturator externus	External rotator	61.31	11.01	1.00	0.00	2.70	5.57
Obturator internus	External rotator	110.29	14.51	1.00	0.00	2.70	7.60
Pectineus	Adductor	89.96	13.21	1.00	0.00	2.70	6.81
Piriformis	External rotator	66.46	12.54	1.00	0.00	2.70	5.30
Psoas minor	Flexor						1.10
Psoas major	Flexor	244.13	25.73	0.50	10.60	3.11	21.48
Quadratus femoris	External rotator	43.81	8.77	1.00	0.00	2.70	4.99
Rectus femoris	Flexor	185.74	31.36	0.21	13.90	2.42	24.54
Sartorius	Flexor	186.40	49.44	0.90	1.30	3.11	4.82
Semimembranosus	Extensor, Internal rotator	317.77	32.46	0.24	15.10	2.61	38.07
Tensor fasciae latae	Abductor	107.76	18.29	1.00	0.00	2.70	5.89

The muscle volume and muscle length were obtained through manual segmentation of the MRI scans. The fibre length to muscle length ratio, pennation angle and sarcomere length were obtained from the literature [26]. For the gemellus, gluteus minimus, obturator externus, obturator internus, pectineus, quadratus femoris and tensor fasciae latae muscles, which have not been reported in the literature [26], the fibre length to muscle length ratio was set to 1.00, the pennation angle was set to 0.00° and the sarcomere length to 2.70 µm, respectively [16], [27]. The psoas minor physiological cross-sectional area (PCSA) was obtained from the literature [24].

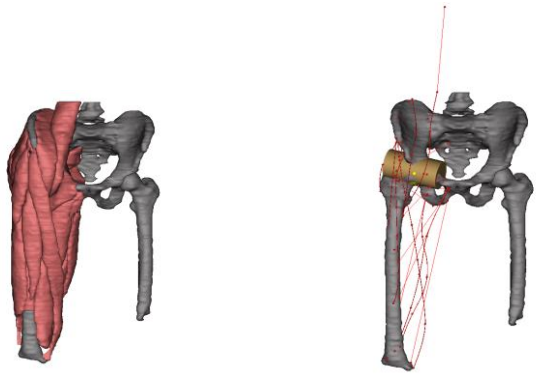

(A) (B)

Fig. 1. Lower limb anatomy of a representative subject (one limb of a bilateral above-knee amputee): (A) pelvis, femoral remnants and muscle 3D reconstruction. (B) muscle lines-of-action (red), hip joint centre (yellow point), wrapping object (yellow cylinder).

C. Musculoskeletal modelling and data analysis

Internal forces during the gait trials were quantified using Freebody v2.1, a segment based musculoskeletal model [28], [29] adapted for above and through-knee amputee use. The model has four rigid segments: pelvis, thigh, shank and foot; the stump, stump liner and prosthetic socket were combined to model the thigh segment. The pelvis and thigh segments are articulated at the hip joint (spherical joint with 3 degrees of freedom) and actuated by 92 muscle elements, illustrated in Fig. 2. Inverse kinematics and inverse dynamics simulations were used to obtain moments at the hip joint for the recorded gait trials. The segments' locations and orientations are derived from the coordinates of the reflective markers placed on the previously presented anatomical landmarks (Section II.A).

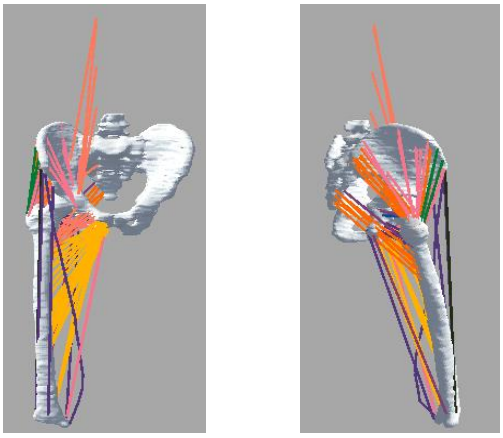

(A) (B)

Fig. 2. Musculoskeletal model of a trans-femoral amputee. (A) Frontal view (B) Lateral view.

The one-step static load sharing optimisation algorithm, presented in (2), was implemented to compute the forces in each muscle element (F_i) and the resultant contact force at the hip joint. The algorithm aims to minimize the sum of cubed muscle activations (J) [30]. Each muscle element's maximum force, $F_{max,i}$, was computed as the multiplication of the muscle element PCSA, the PCSA multiplier and the maximum muscle stress, 31.39 N/cm^2 [31]. Muscles that cross the absent joint were removed or adjusted for their new insertions and their contribution to the static optimisation was adjusted accordingly. The prosthesis' contribution to the net joint moment was computed using inverse dynamics. The torques were presented at the midpoint between the medial and lateral malleoli on the prosthetic foot and between the medial and lateral epicondyles on the prosthetic knee, respectively.

$$\min(J) = \sum_{i=1}^{92} \left(\frac{F_i}{F_{max,i}}\right)^3 \quad (2)$$

Anthropometry and body segment parameters (mass, centre of mass location, moment of inertia) served as input to the musculoskeletal model. DeLeva calculations [32] were used to determine the pelvic and stump segment parameters. The stump length was measured from the MRI scans as the distance from the hip joint centre to the most distal point on the residual limb. The mass of the stump was obtained by multiplying the stump volume (rendered 3D geometry from the MRI scans) by density (1.42 g/cm^3 for bone, 1.03 g/cm^3 for soft tissue [33]). This calculation was made under the assumption that the body is formed of two parts, bone and soft tissue, both of uniform densities [34]. The prosthetic component parameters were determined using a reaction board method [35] and moment equilibrium was used to determine the centre of mass location for the prosthetic components. The total moment of inertia of the thigh segment was obtained by adding the moment of inertia of the stump to that of the prosthetic components (liners, socket, connectors) using the Huygens-Steiner parallel axis theorem [36].

The atlas consists of a total of 18 subject-specific anatomical models, where each subject-specific model is composed of the subject's marker trajectory, force plate and MRI-based anatomical data (skeletal geometry and muscle properties). 12 subject-specific models were validated using the recorded EMG signals. The evaluation was performed by comparing the EMG data and the predicted muscle activations. For each model, EMG data were normalized to the maximum recording in the gait trial to obtain activation values from 0 to 1. The predicted muscle activations were also defined from 0 to 1 as the predicted muscle force normalized by the maximum force in the gait trial. The Sprague and Geers (S&G) metric [37], defined in Table III, was used to quantify the magnitude (M), phase (P) and combined (C) errors, where the combined measure accounts for both M and P errors.

TABLE III
SPRAGUE AND GEERS METRIC INTERPRETATION [15]

Error interval	Similarity
0 – 0.15	excellent
0.15 – 0.30	very good
0.30 – 0.45	good
0.45 – 0.60	moderate
> 0.60	none

Whereas 12 limb-specific models (6 subjects × 2 limbs) were validated, the overall scaling process included all 18 models (9 subjects × 2 limbs). The two limbs (left and right sides) for

each study participant were analysed separately, since the used musculoskeletal model simulates unilateral models only. Therefore, each limb in the atlas had a customised model and 17 further models created through linear scaling to the remaining anatomical datasets. The linear scaling factors were the ratios of intersegmental length and width measured from the subject in the static trial to the intersegmental length and width in the dataset used for scaling. These factors were used to scale the muscle lines-of-action, wrapping object parameters and hip joint rotation centre. In total, there were 972 simulations (18 models x 18 anatomical datasets x 3 gait trials). Fig. 3 presents the cross-validation process for one model, where M1 represents the anthropometric, force plate and marker trajectory data and A_i represents the i^{th} anatomical dataset.

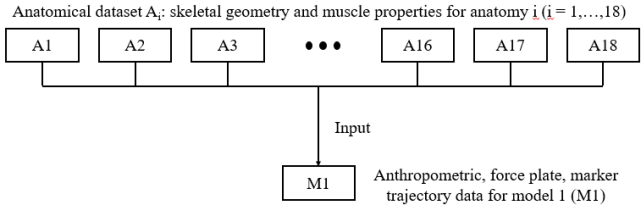

Fig. 3. Musculoskeletal simulation pipeline for model 1. The limb-specific model is formed of model 1's anatomy (A1) and anthropometric, force plate and marker trajectory data (M1). The anatomical datasets A2-A18 serve as input to the musculoskeletal model consisting of model M1's data, therefore completing the remaining 17 linearly scaled models.

The computed muscle and hip joint contact forces were expressed as a gait cycle percentage from 0% at heel strike to 100% at the consecutive heel strike in intervals of 1% and averaged over the three trials. Muscles were grouped based on their function into 6 categories: adductors, abductors, extensors, flexors, internal rotators and external rotators. The total force in one muscle group during walking was calculated by adding the forces for all muscles that possess the corresponding function. The root-mean-square difference (RMSD, Equation 3 [16]), normalized by the mean force in the gait cycle (as presented in a previous study [16]) from the subject-specific model ($\overline{F_{ss}}$), was used to quantify the differences between the scaled and subject-specific model output for the hip joint contact and muscle group forces, where the subject-specific model output was considered ground truth. F_{ss}^{i} and F_{sm}^{i} represent the forces from the subject-specific and scaled model output, respectively, for each time frame (i).

$$\mathrm{RMSD} = \frac{\sqrt{\frac{\sum_{i=0}^{100}(F_{ss}^{i} - F_{sm}^{i})^2}{100}}}{\overline{F_{ss}}} \times 100\ (\%) \quad (3)$$

To assess the dependency of the musculoskeletal model predictions on the amputee anatomy, the effects of the following anthropometric parameters were investigated: mass without prosthetic components, intact mass and body mass index (BMI) calculated using the intact mass [18], pre-amputation height, stump length (distance from the hip joint centre to the distal end of the residual limb), pelvis width (distance between the left and right anterior iliac spine anatomical landmarks), stump length to pelvis width ratio and prosthesis type parameter, which was assigned a 1 if the residual limb was fitted with a stubby prosthesis and 0 otherwise. The choice of mass and height was based on the previous finding that muscle properties scale with these measurements [25]. The stump length is an indication of the residual muscle volume. Differences in BMI and pelvis width have been shown to introduce significant differences in force predictions for able-body lower limb models [16]. Finally, it was hypothesised that differences in fitted prosthetic components introduce discrepancies in force predictions.

Regression analysis was used to identify relationships between differences in individual anthropometric parameters and RMSD values for the hip joint and muscle forces in the presence of all investigated parameters. The final multiple linear regression models were identified using stepwise regression analysis. Three regression models were developed, each aiming to minimize the errors in: 1. hip joint contact forces 2. muscle forces and 3. combined hip joint and muscle forces (for which a compound measure was created by obtaining the average of the force errors across all muscle groups and then averaging it with the errors in the predicted hip joint contact forces). The combined regression model was created in order to equally account for the accuracy in both muscle and hip joint contact force predictions [15]. To assess the effect of the weighting distribution of the hip and muscle force errors in the combined regression model, all weights from 0% to 100% were considered. The three models were then used to identify the model in the anatomical atlas with the closest predictions to the subject-specific model output. To assess the robustness of the models, the variance was checked for normal distribution by plotting the histogram of residuals.

III. RESULTS

A. *Validation of subject-specific models*

Fig. 4 compares the normalized predicted muscle forces to the normalized EMG curve for one representative model.

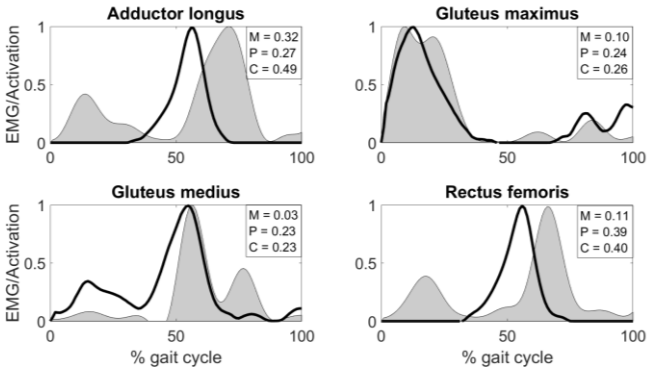

Fig. 4. Predicted muscle activations (solid line) and normalized EMG data (shaded area) for the adductor longus, gluteus maximus, gluteus medius and rectus femoris muscles for a representative model. M, P and C represent the magnitude, phase and combined errors, respectively, quantified using the Sprague and Geers metric.

The observed differences between the predicted and recorded muscle activations for 12 subject-specific models are shown in

Table IV. The magnitude errors ranged from 0.13 (±0.10) for gluteus maximus to 0.24 (±0.11) for adductor longus. The phase errors ranged from 0.23 (±0.09) for gluteus maximus to 0.34 (±0.06) for rectus femoris. Finally, the combined errors varied from 0.28 (±0.10) for gluteus maximus to 0.42 (±0.11) for the adductor longus muscle. All results were excellent, very good or good, demonstrating that the models were able to predict muscle activations.

TABLE IV
ABSOLUTE VALUES OF THE SPRAGUE AND GEERS METRIC MAGNITUDE (M), PHASE (P) AND COMBINED (C) ERRORS BETWEEN THE EMG SIGNALS AND SUBJECT-SPECIFIC MODEL MUSCLE ACTIVITY PREDICTIONS FOR THE ADDUCTOR LONGUS, GLUTEUS MAXIMUS, GLUTEUS MEDIUS AND RECTUS FEMORIS. THE ERRORS ARE AVERAGED ACROSS ALL MODELS (N = 12). C < 0.15 INDICATES EXCELLENT, 0.15 < C < 0.30 VERY GOOD AND 0.30 < C < 0.45 GOOD SIMILARITY

S&G metric/Muscle	M	P	C
Adductor longus	0.24±0.11	0.33±0.09	0.42±0.11
Gluteus maximus	0.13±0.10	0.23±0.09	0.28±0.10
Gluteus medius	0.14±0.13	0.27±0.05	0.33±0.07
Rectus femoris	0.21±0.10	0.34±0.06	0.41±0.09

B. Predictors of discrepancies in muscle and hip joint contact forces

The RMSD values, normalized by the maximum force from the subject-specific model, were analysed in relation to percentage differences in anthropometric parameters from the subject-specific dataset. Table V presents the correlations between differences in each individual anthropometric parameter and RMSD values, in the presence of all investigated parameters, for the hip joint, muscle and 50:50 combined hip joint contact and muscle forces.

TABLE V
CORRELATIONS BETWEEN DIFFERENCES IN PREDICTED HIP JOINT CONTACT FORCES, MUSCLE FORCES AND PERCENTAGE DIFFERENCES IN ANTHROPOMETRIC PARAMETERS FROM THE SUBJECT-SPECIFIC MODEL

	Hip joint		Muscle groups		Hip joint & Muscle groups	
Parameter	R^2 (%)	p value	R^2 (%)	p value	R^2 (%)	p value
ΔPW[a]	9.01	<0.001	9.87	<0.001	12.12	<0.001
ΔBMI	7.12	<0.001	3.89	<0.001	5.87	<0.001
Δintact mass	4.22	<0.001	5.71	<0.001	6.65	<0.001
Δintact height	2.99	0.0018	5.09	<0.001	5.63	<0.001
Δmass (no pr.)	2.06	0.0096	4.13	<0.001	4.40	<0.001
Δprosthesis	1.57	0.02	0.51	0.20	0.04	0.71
Δstump length	0.04	0.73	3.76	<0.001	2.34	0.0058
Δratio[b]	0.01	0.85	3.69	<0.001	2.38	0.0054

[a] PW represents the pelvis width.
[b] ratio represents the stump length to pelvis width ratio.

Scaling to the available models in the atlas introduced RMSD values in hip joint force predictions varying from 5.7% to 102.1%. Significant correlations ($p < 0.05$) were identified between discrepancies in internal force predictions and percentage differences in all anthropometric parameters, with the exception of the stump length and stump length to pelvis width ratio for the hip joint contact force and prosthesis type for the muscle and combined forces. Differences in pelvis width presented the strongest and most significant correlation with discrepancies in hip joint contact, muscle and combined forces, explaining 9.0% ($p < 0.001$), 9.9% ($p < 0.001$) and 12.1% ($p < 0.001$), respectively, of the total variability.

Table VI presents the three identified multiple linear regression models, which aim to minimize the differences in the hip joint, muscle groups and overall internal force predictions.

TABLE VI
MULTIPLE LINEAR REGRESSION MODELS RELATING PERCENTAGE DIFFERENCES IN SIGNIFICANT ANTHROPOMETRIC PREDICTORS TO RMSD VALUES IN PREDICTED INTERNAL FORCES

Hip joint contact forces
min(RMSD) = min(11.98+3.26×ΔPW+1.91×ΔBMI-0.26×ΔBMI×ΔPW)
R^2 = 27.47%, adjusted R^2 = 26.79%, $p < 0.001$

Predictor	Coefficient	Standard error	p value	95% CI[a]
intercept	11.98	1.96	<0.001	(8.13 15.84)
ΔPW[b]	3.26	0.35	<0.001	(2.58 3.95)
ΔBMI	1.91	0.22	<0.001	(1.47 2.35)
ΔBMI × ΔPW	-0.26	0.03	<0.001	(-0.32 -0.20)

Muscle forces
min(RMSD) = min(36.82+6.55×ΔPW+2.85×ΔBMI+0.29×Δratio-0.38×ΔBMI×ΔPW)
R^2 = 19.76%, adjusted R^2 = 18.76%, $p < 0.001$

Predictor	Coefficient	Standard error	p value	95% CI
intercept	36.82	5.93	<0.001	(25.15 48.49)
ΔPW	6.55	1.00	<0.001	(4.59 8.51)
ΔBMI	2.85	0.64	<0.001	(1.58 4.11)
Δratio[c]	0.29	0.08	<0.001	(0.13 0.45)
ΔBMI × ΔPW	-0.38	0.09	<0.001	(-0.56 -0.20)

50:50 combined muscle and hip joint contact forces
min(RMSD) = min(24.82+4.93×ΔPW+2.39×ΔBMI+0.13×Δratio-0.32×ΔBMI×ΔPW)
R^2 = 25.55%, adjusted R^2 = 24.62%, $p < 0.001$

Predictor	Coefficient	Standard error	p value	95% CI
intercept	24.82	3.49	<0.001	(17.96 31.68)
ΔPW	4.93	0.59	<0.001	(3.78 6.08)
ΔBMI	2.39	0.38	<0.001	(1.65 3.14)
Δratio	0.13	0.05	0.0098	(0.03 0.22)
ΔBMI × ΔPW	-0.32	0.05	<0.001	(-0.43 -0.22)

[a] CI represents the confidence intervals.
[b] PW represents the pelvis width.
[c] ratio represents the stump length to pelvis width ratio.

Stepwise multiple regression analysis identified significant predictors of RMSD values in force predictions to be: differences in pelvis width (coefficient B = 3.26, $p < 0.001$), BMI (B = 1.91, $p < 0.001$) and their multiplication (B = -0.26, $p < 0.001$) for the hip joint contact forces; differences in pelvis width (B = 6.55, $p < 0.001$), BMI (B = 2.85, $p < 0.001$), their multiplication (B = -0.38, $p < 0.001$) and stump length to pelvis width ratio (B = 0.29, $p < 0.001$) for the muscle forces; differences in pelvis width (B = 4.93, $p < 0.001$), BMI (B = 2.39, $p < 0.001$), their multiplication (B = -0.32, $p < 0.001$) and stump length to pelvis width ratio (B = 0.13, $p = 0.0098$) for the combined forces. The inclusion of the remaining parameters in the multiple regression models increased the R^2

value by 1.6% for the hip joint contact forces, 0.8% for the muscle groups forces and 0.7% for the overall internal forces.

The muscle force regression equation led to the choice of the same anatomy to be used from the atlas as the hip joint force equation in 15 cases out of the total of 18, whereas the 50:50 combined hip and muscle force regression equation led to the choice of the same anatomy as the hip joint force model. All combined models with a weighting of muscle forces of less than 50% resulted in the same anatomy choice. Table VII shows the RMSD values in hip joint contact forces (one of our key musculoskeletal health-related variables) resulting from scaling to the closest anatomical model in the atlas using the 50:50 combined, hip joint and muscle forces regression models.

TABLE VII
DIFFERENCES IN HIP JOINT CONTACT FORCE PREDICTIONS BETWEEN THE SCALED MODEL OUTPUT AND THE SUBJECT-SPECIFIC MODEL OUTPUT FOR ALL MODELS (N = 18) USING DIFFERENT REGRESSION MODELS. THE HIP JOINT AND 50:50 COMBINED MODELS LED TO THE CHOICE OF THE SAME ANATOMICAL DATASET TO USE FROM THE ATLAS

Regression model	Mean RMSD[a]	SD[b]	Median RMSD	Minimum RMSD	Maximum RMSD
50:50 combined	18.03%	±5.84%	16.77%	10.97%	29.03%
Hip joint	18.03%	±5.84%	16.77%	10.97%	29.03%
Muscle	20.07%	±8.48%	17.65%	10.97%	40.71%

[a] RMSD represents the root-mean-square difference.
[b] SD represents the standard deviation.

IV. DISCUSSION

A. Validation of subject-specific models

The accuracy of 12 subject-specific models was evaluated by comparing the recorded and predicted muscle activations from the musculoskeletal model. The Sprague and Geers metric was used to quantify the magnitude, phase and combined errors. According to the metric, very good similarity was observed between the predicted and recorded gluteus maximus activations, since the combined error was less than 0.30. With combined errors of less than 0.45, there was good similarity for the gluteus medius, rectus femoris and adductor longus muscles. These findings compare well to able bodied lower limb models, with combined magnitude and phase S&G errors of 0.31 (±0.10) and 0.44 (±0.12) for the gluteus medius and rectus femoris muscles, respectively [16].

The sub-optimal placement of the EMG sensors, combined with possible cross talk between adjacent muscles, may have reduced the quality of the received signal. The electromechanical delay between the force onset and EMG signal [38] was not accounted for in the musculoskeletal model, as the magnitude of the delay is not known in atrophied muscles of amputees. Phase delays were most visible in the rectus femoris and adductor longus activity, with S&G metric phase errors of 0.34 (±0.06) and 0.33 (±0.09), respectively. Previous studies have implemented the EMG delay [21]. However, as an accurate quantification of the delay was not possible for the current cohort, no correction was applied in this study. Use of prosthetic sockets with cut-outs, which allow for the optimal EMG placement recommended in the literature [22], would increase the fidelity of the model validation. However, given that all magnitude, phase and combined S&G errors were less than 0.45, therefore indicating good similarity between the recorded and predicted muscular activations, the validation of the 12 subject-specific models was considered successful. The remaining 6 models could not be validated due to the inability to optimally position the EMG sensors on the residual limbs.

B. Predictors of discrepancies in hip joint contact forces

The hip joint contact force is considered a key variable as its magnitude is linked to the likelihood of developing musculoskeletal diseases such as osteoarthritis and osteopenia. When direct measurements, such as instrumented implants, are not available, customised musculoskeletal modelling using linear scaling can enable the quantification of internal forces [12]. However, linear scaling to a generic lower limb amputee model can produce significant inaccuracies in the predicted hip joint forces since it does not account for anatomical inter-individual variability [14]. This is confirmed by the large range of RMSD values (from 5.7% to 102.1%) between the hip joint contact forces from the scaled and subject-specific model output. The differences in pelvis width and BMI were the primary predictors of RMSD in hip joint forces, each explaining 9.0% ($p < 0.001$) and 7.1% ($p < 0.001$) of the total variability, respectively. Moreover, it was noted that the mass and height differences account for inaccuracies in the hip joint forces output. The fact that the mass and inertial properties of the intact segments were not scaled in a subject-specific manner, but rather generically through the DeLeva regression equations [32], may have contributed to inaccuracies in hip joint contact forces. Future work should consider scaling of these parameters.

Unexpectedly, the percentage differences in stump length presented no significant correlation with discrepancies in hip joint forces. This wide variability among traumatic amputees is caused by different factors. Firstly, the muscle re-insertion locations differ from subject to subject and the surgical procedure introduces the possibility of shorter stumps having stronger musculature than longer residual limbs through the preservation of muscle tension during reattachment [39]. Secondly, the rehabilitation and prosthetic training process greatly influences the amputee's musculoskeletal function – different training protocols can improve the functional capacity of different muscle groups. As a result, amputees adopt very distinct movement strategies in order to maximise comfort, performance, endurance, or minimise energy consumption and pain.

The final multiple linear regression model described 27.5% (adjusted $R^2 = 26.8\%$, $p < 0.001$) of the differences in hip joint contact forces. The anthropometric parameters, which were not included in the multiple regression model, accounted for less than 2% of the variability, suggesting that the pelvis width

and BMI are the most significant parameters that have to be considered during the analysis of hip joint contact forces from musculoskeletal modelling using a non-subject-specific anatomical dataset. Previous work identified the differences in limb length ($p < 0.001$), mass ($p = 0.033$) and gender ($p = 0.039$) to be the most significant indicators of discrepancies in predicted hip joint forces during gait of able-bodied individuals, the final regression model accounting for 33.3% of the variance of differences in computed forces [16]. The lower proportion of variance explained by the amputee model may be justified by the wider anatomical variability found in this group compared to able-bodied subjects.

C. Predictors of discrepancies in muscle forces

The primary predictor of differences in computed muscle forces was the difference in pelvis width ($R^2 = 9.9\%$, $p < 0.001$), as was the case for the predicted hip joint contact forces, and the intact mass and height were the following most significant predictors. Muscle properties have been shown to scale with subject mass and limb length [25]. In this study, it was found that the percentage differences in the pre- and post-amputation mass accounted for 5.7% ($p < 0.001$) and 4.1% ($p < 0.001$), respectively. The percentage differences in the pre-injury height (proportional to intact limb length) accounted for 5.1% ($p < 0.001$) of the variability and the stump length for 3.8% ($p < 0.001$). These numbers are significant when compared to the degree of variability that the pelvis width is accounting for. This study's cohort of amputees presents a small range (1.71 - 1.86 m) of pre-injury height values. With a larger variability, a stronger correlation may be observed between the discrepancies in pre-injury height values and differences in internal force predictions.

The multiple regression model described 19.8% (adjusted $R^2 = 18.8\%$, $p < 0.001$) of the variance of discrepancies in muscle force predictions. The model identified the same anthropometric parameters as the hip joint model to be significant predictors of discrepancies in force predictions (differences in pelvis width and BMI), with the addition of differences in the stump length to pelvis width ratio parameter, which did not significantly improve the R^2 value of the hip joint contact force regression model.

D. Predictors of discrepancies in muscle and hip joint contact forces

The final 50:50 combined multiple linear regression model accounted for 25.5% (adjusted 24.6%, $p < 0.001$) of the variance of RMSD in muscle and hip joint contact forces. The addition of the remaining parameters in the multiple regression model increased the R^2 value by less than 1%, demonstrating the pelvis width, BMI and stump length to pelvis width ratio to be the most significant anthropometric parameters that have to be considered during musculoskeletal modelling using non-subject-specific geometries. Scaling using the closest model, identified by the multiple linear regression model, introduced an average RMSD value of 18% in the predicted hip joint loading, which is the key variable. This RMSD value equates to 0.38 bodyweight difference for the hip joint contact forces and is at the lower end of the total range of errors obtained from linear scaling to one model (5.7 – 102.1%). A previous study [16] found that linear scaling of able-bodied lower limb models to the closest anatomical dataset produced an average error of 16% in joint contact force calculations. This difference of 2% may be attributed to the wider anthropometric and anatomical variability in amputees than able-bodied individuals.

The choice of which regression model to use is based on both the purpose of the model (which application is to be considered), and the differences in errors. As the hip joint contact force is heavily dependent on the estimated muscle forces, an argument can be made to select the model only based on muscle forces. However, the hip joint regression model had the strongest explanatory and statistical power of all presented regression models and the musculoskeletal model used in this study (Freebody v2.1) was validated for joint contact forces from instrumented implant measurements [16]. The R^2 value of the 50:50 combined model was 2% lower than of the hip joint model and both models led to the same choice of anatomical dataset to scale to. The difference in R^2 value between the two extreme cases with 0% and 100% weighting of muscle force errors in the combined model was 8%.

The muscle force regression equation led to the choice of the same anatomy to be used from the atlas as the hip joint and 50:50 combined models in 83.3% of the cases. Scaling to the closest dataset, identified by the muscle regression model, increased the errors in the hip joint force predictions, a key variable for the general assessment of musculoskeletal health, by 2% when compared to the use of the combined regression model. In order to accurately predict hip joint contact forces, as well as muscle forces, it is recommended that the combined regression model, with equal weighting distribution, is used to choose the closest anatomical dataset to scale to.

The full anatomical atlas, consisting of 18 datasets (bone .stl files, joint, muscle and wrapping object parameters, muscle lines-of-action, bony landmarks coordinates), is available at http://www.msksoftware.org.uk.

E. Limitations

The static optimisation algorithm implemented in this study is based on the minimisation of energy expenditure, as lower limb amputees have been shown to walk at a self-selected speed which aims to minimize the energy expenditure per metre walked [40]. This cost function has previously been validated in the musculoskeletal modelling framework for transtibial amputee and able-bodied gait [4], [29] and so, it was assumed that this algorithm also applies for through-knee and trans-femoral amputees. However, this young and motivated cohort of military bilateral lower limb amputees may have different objectives and some prior work shows that amputees walk at speeds different from the energy efficient ones [41]. Therefore, maximisation of performance or

stability, minimisation of pain or impact at heel strike should be considered.

Secondly, the prosthetic socket, stump liner and the residual limb were modelled as a single rigid segment, without considering the angular and axial movement at the socket-stump interface [42]. Although these movements are typically very small, in the order of 12° and 36 mm [42], the effect of this simplification in the model should be investigated.

The current study analysed gait only and did not include other activities of daily living. Therefore, using the identified linear regression models in musculoskeletal modelling of other motion tasks may lead to errors in model predictions. Furthermore, the identified multiple linear regression models only apply to musculoskeletal modelling using the linear scaling law and different scaling methods may change the regression models. Also, non-linear scaling, based on a morphing technique, has been shown to improve the model predictions when compared to the ones obtained through linear scaling [43]. However, the majority of lower limb musculoskeletal models utilise linear scaling. As a future improvement, the non-linear method could be implemented on the available dataset to generate outputs with increased accuracy.

Muscle force predictions have been shown to be sensitive to the variation in muscle properties [44], [45]. In this study, the pennation angle, fibre length to muscle length ratio and sarcomere length parameters were not subject-specific, but instead obtained from studies based on elderly cadavers [26], [27]. As these values cannot be acquired from imaging scans, assigning these parameter's values from in vivo cadaveric studies is common in the literature [15], [16]. Furthermore, the muscle moment arms were defined using imaging scans capturing the standard position of the subjects in the MRI scanner and so, changes in muscle moment arms during dynamic conditions were not included in the model.

Finally, this anatomical atlas consists of only male subjects and does not account for gender differences in pelvic shape [46] and distal femur [47] (in the case of through-knee amputees). A previous study, which used an anatomical atlas to improve scaling of musculoskeletal lower limb modelling for able-bodied individuals [16], found that gender differences improve the regression fit of RMSDs in hip joint forces by 2%. Future work could develop anatomical datasets for female subjects in order to account for gender differences.

V. CONCLUSION

This study presents the first EMG-validated musculoskeletal model for bilateral through- and above-knee amputees. An anatomical atlas of 18 datasets is presented and used to show that linear scaling to the anatomy with anthropometric similarity can accurately predict muscle and joint contact forces, thus enabling such models to be used pervasively without recourse to expensive imaging-derived anatomies.

REFERENCES

[1] D. S. Edwards *et al*, "What is the magnitude and long-term economic cost of care of the british military Afghanistan amputee cohort?," *Clin. Orthop. Relat. Res.*, vol. 473, no. 9, pp. 2848–2855, 2015.

[2] H. L. Jarvis *et al*, "Temporal spatial and metabolic measures of walking in highly functional individuals with lower limb amputations," *Arch. Phys. Med. Rehabil.*, vol. 98, no. 7, pp. 1389–1399, 2017.

[3] H. L. Jarvis *et al*, "Can high-functioning amputees with state-of-the-art prosthetics walk normally? A kinematic and dynamic study of 40 individuals," *Ann. Phys. Rehabil. Med.*, pp. 4–11, 2020.

[4] Z. Ding *et al*, "Higher knee contact forces might underlie increased osteoarthritis rates in high functioning amputees: A pilot study," *J. Orthop. Res.*, no. May, pp. 1–11, 2020.

[5] D. C. Norvell *et al*, "The prevalence of knee pain and symptomatic knee osteoarthritis among veteran traumatic amputees and nonamputees," *Arch. Phys. Med. Rehabil.*, vol. 86, no. 3, pp. 487–493, 2005.

[6] M. J. Burke *et al*, "Bone and joint changes in lower limb amputees," *Ann. Rheum. Dis.*, vol. 37, no. 3, pp. 252–254, 1978.

[7] P. J. Rush *et al*, "Osteopenia in patients with above knee amputation," *Arch. Phys. Med. Rehabil.*, vol. 75, no. 1, pp. 112–115, 1994.

[8] P. L. Ephraim *et al*, "Phantom pain, residual limb pain, and back pain in amputees: Results of a national survey," *Arch. Phys. Med. Rehabil.*, vol. 86, no. 10, pp. 1910–1919, 2005.

[9] E. Isakov *et al*, "Trans-tibial amputee gait: Time-distance parameters and EMG activity," *Prosthet. Orthot. Int.*, vol. 24, no. 3, pp. 216–220, 2000.

[10] S. M. H. J. Jaegers *et al*, "Prosthetic gait of unilateral transfemoral amputees: A kinematic study," *Arch. Phys. Med. Rehabil.*, vol. 76, no. 8, pp. 736–743, 1995.

[11] G. D. Summers *et al*, "Foot loading characteristics of amputees and normal subjects," *Prosthet. Orthot. Int.*, vol. 11, no. 1, pp. 33–39, 1987.

[12] D. J. Cleather and A. M. J. Bull, "The development of lower limb musculoskeletal models with clinical relevance is dependent upon the fidelity of the mathematical description of the lower limb. Part 2: Patient-specific geometry," *Proc. Inst. Mech. Eng. Part H J. Eng. Med.*, vol. 226, no. 2, pp. 133–145, 2012.

[13] B. L. Kaptein and F. C. T. Van Der Helm, "Estimating muscle attachment contours by transforming geometrical bone models," *J Biomech*, vol. 37, pp. 263–273, 2004.

[14] G. N. Duda *et al*, "Variability of femoral muscle attachments," *J. Biomech.*, vol. 29, no. 9, pp. 1185–1190, 1996.

[15] C. Klemt *et al.*, "Anthropometric scaling of anatomical datasets for subject-specific musculoskeletal modelling of the shoulder," *Ann. Biomed. Eng.*, vol. 47, no. 4, pp. 924–936, 2019.

[16] Z. Ding *et al*, "Improving musculoskeletal model scaling using an anatomical atlas: the importance of gender and anthropometric similarity to quantify joint reaction forces," *IEEE Trans. Biomed. Eng.*, vol. 66, no. 12, pp. 1–13, 2019.

[17] L. Scheys *et al*, "Calculated moment-arm and muscle-tendon lengths during gait differ substantially using MR based versus rescaled generic lower-limb musculoskeletal models," *Gait Posture*, vol. 28, no. 4, pp. 640–648, 2008.

[18] A. H. Tzamaloukas *et al*, "Body mass index in amputees," *J. Parenter. Enter. Nutr.*, vol. 18, no. 4, pp. 355–358, 1994.

[19] L. D. Duffell *et al*, "Comparison of kinematic and kinetic parameters calculated using a cluster-based model and Vicon's plug-in gait," *Proc. Inst. Mech. Eng. Part H J. Eng. Med.*, vol. 228, no. 2, pp. 206–210, 2014.

[20] B. Yu *et al*, "Estimate of the optimum cutoff frequency for the Butterworth low-pass digital filter," *J. Appl. Biomech.*, vol. 15, no. 3, pp. 318–329, 1999.

[21] E. M. Arnold *et al*, "How muscle fiber lengths and velocities affect muscle force generation as humans walk and run at different speeds," *J. Exp. Biol.*, vol. 216, no. 11, pp. 2150–2160, 2013.

[22] A. O. Perotto, *Anatomical guide for the electromyographer: the limbs and trunk*. Charles C Thomas Publisher, 2011.

[23] N. Mitsiopoulos *et al*, "Cadaver validation of skeletal muscle measurement by magnetic resonance imaging and computerized tomography," *J. Appl. Physiol.*, vol. 85, no. 1, pp. 115–122, 1998.

[24] M. D. Klein Horsman *et al*, "Morphological muscle and joint parameters for musculoskeletal modelling of the lower extremity," *Clin. Biomech.*, vol. 22, no. 2, pp. 239–247, 2007.

[25] G. G. Handsfield *et al*, "Relationships of 35 lower limb muscles to height and body mass quantified using MRI," *J. Biomech.*, vol. 47, no. 3, pp. 631–638, 2014.
[26] S. R. Ward *et al*, "Are current measurements of lower extremity muscle architecture accurate?," *Clin. Orthop. Relat. Res.*, vol. 467, no. 4, pp. 1074–1082, 2009.
[27] R. L. Lieber *et al*, "In vivo measurement of human wrist extensor muscle sarcomere length changes," *J. Neurophysiol.*, vol. 71, no. 3, pp. 874–881, 1994.
[28] D. J. Cleather and A. M. J. Bull, "The development of a segment-based musculoskeletal model of the lower limb: Introducing FREEBODY," *R. Soc. Open Sci.*, vol. 2, no. 6, 2015.
[29] Z. Ding *et al*, "In vivo knee contact force prediction using patient-specific musculoskeletal geometry in a segment-based computational model," *J. Biomech. Eng.*, vol. 138, no. 2, pp. 1–9, 2016.
[30] R. D. Crowninshield and R. A. Brand, "A physiologically based criterion of muscle force prediction in locomotion," *J Biomech*, vol. 14, no. 11, pp. 793–801, 1981.
[31] G. T. Yamaguchi, *Dynamic modelling of musculoskeletal motion: a vectorized approach for biomechanical analysis in three dimensions*. Springer Science & Business Media, 2005.
[32] P. De Leva, "Adjustments to Zarsiorsky-Seluyanov`s segment inertia parameters," *Int. J. Imaging Syst. Technol.*, vol. 29, no. 9, pp. 1223–1230, 1996.
[33] D. R. White *et al*, "Average soft-tissue and bone models for use in radiation dosimetry," *Br. J. Radiol.*, vol. 60, pp. 907–13, 1987.
[34] G. Valente *et al.*, "Are subject-specific musculoskeletal models robust to the uncertainties in parameter identification?," *PLoS One*, vol. 9, no. 11, 2014.
[35] J. D. Smith *et al*, "Oscillation and reaction board techniques for estimating inertial properties of a below-knee prosthesis," *J. Vis. Exp.*, vol. 87, pp. 1–15, 2014.
[36] A. E. Haas, *Introduction to theoretical physics*. Constable Limited, 1928.
[37] H. Sarin *et al*, "Comparing time histories for validation of simulation models: Error measures and metrics," *J. Dyn. Syst. Meas. Control. Trans. ASME*, vol. 132, no. 6, pp. 1–10, 2010.
[38] P. R. Cavanagh and P. V. Komi, "Electromechanical delay in human skeletal muscle under concentric and eccentric contractions," *Eur. J. Appl. Physiol. Occup. Physiol.*, vol. 42, no. 3, pp. 159–163, 1979.
[39] E. C. Ranz *et al*, "The influence of limb alignment and transfemoral amputation technique on muscle capacity during gait," *Comput. Methods Biomech. Biomed. Engin.*, vol. 20, no. 11, pp. 1167–1174, 2017.
[40] V. T. Inman, "Human locomotion," *Can. Med. Assoc. J.*, vol. 94, no. 20, p. 1047, 1966.
[41] S. M. H. J. Jaegers *et al*, "The relationship between comfortable and most metabolically efficient walking speed in persons with unilateral above-knee amputation," *Arch. Phys. Med. Rehabil.*, vol. 74, no. 5, pp. 521–525, 1993.
[42] J. Tang *et al.*, "Characterisation of dynamic couplings at lower limb residuum/socket interface using 3D motion capture," *Med. Eng. Phys.*, vol. 37, no. 12, pp. 1162–1168, 2015.
[43] D. Nolte *et al*, "Non-linear scaling of a musculoskeletal model of the lower limb using statistical shape models," *J. Biomech.*, vol. 49, no. 14, pp. 3576–3581, 2016.
[44] V. Carbone *et al*, "Sensitivity of subject-specific models to Hill muscle – tendon model parameters in simulations of gait," *J. Biomech.*, vol. 49, no. 9, pp. 1953–1960, 2016.
[45] M. Zuk *et al*, "Influence of uncertainty in selected musculoskeletal model parameters on muscle forces estimated in inverse dynamics-based static optimization and hybrid approach," *J. Biomech. Eng.*, vol. 140, no. 12, pp. 1–12, 2018.
[46] I. Nakahara *et al*, "Gender differences in 3D morphology and bony impingement of human hips," *J. Orthop. Res.*, vol. 29, no. 3, pp. 333–339, 2011.
[47] F. M. Griffin *et al*, "Anatomy of the epicondyles of the distal femur," *J. Arthroplasty*, vol. 15, no. 3, pp. 354–359, 2000.